GFDM Frame Design for Low-latency Industrial Networks

Julius Ssimbwa, Byungju Lim, and Young-Chai Ko

***Abstract*—This paper proposes a short packet GFDM-based physical (PHY) layer for industrial wireless networks to reduce latency. In our proposed PHY layer, the conventional OFDM scheme used in the data field of IEEE 802.11 WLAN standards is replaced by GFDM. The preamble size is also reduced from 10 symbols to 1 symbol. Furthermore, the fields of the overall packet structure are optimized in terms of total number of subcarriers and cyclic prefix length. Additionally, a noise-free GFDM scheme is subjected to concatenated channel coding to minimize error rate. Through simulation, packet transmission time is reduced by about $40 \sim 72\%$ compared to the OFDM-based PHY layer while achieving a PER of order 10^{-3}. The obtained results show that the GFDM-based PHY layer outperforms its counterpart by exhibiting a lower latency and high reliability. This performance renders the GFDM-based (proposed) PHY layer suitable for adoption in the development of wireless networks for latency and reliability constrained industrial applications. It should be noted that the simulations presented in this paper express our first step in the direction of using GFDM for industrial wireless networks to achieve low latency and high reliability. We therefore consider building a fully functional GFDM based-testbed as part of our future work.**

***Index Terms*—Generalized frequency division multiplexing (GFDM), high-performance wireless, IEEE 802.11 WLAN standards, orthogonal frequency division multiplexing (OFDM).**

I. Introduction

OVER the recent years, technological advancement has led to a tremendous development of both industrial and consumer Internet of Things (IoT) applications such as remote control, process automation, etc [1]–[4]. IoT applications seek to improve user experience and high performance connectivity. On the other hand, the insurmountable traffic demand by the ever increasing IoT applications could be overwhelming to the existing cellular network. This will necessitate increased network offloading supported by different networks such as wireless local area networks (WLANs). Consequently, low-cost, bandwidth and power efficient devices will be required, which will lead to implementation complexities of wireless networks [5]–[8]. Moreover, the existing technologies developed to support IoT applications share common weaknesses of low transmission data rates and short range of communication.

Manuscript received December 16, 2021; approved for publication, December 28, 2021. This paper is specially handled by EIC and Division Editor with the help of three anonymous reviewers in a fast manner.

This work was supported by the National Research Foundation of Korea (NRF) grant funded by the Korea government (MSIT)(NRF-2020R1A4A1019628).

Y.-C. Ko is corresponding author.

The authors are with the School of Electrical Engineering, Korea University, Seoul 02841, South Korea, email: {kayjulio, limbj93, koyc}@korea.ac.kr.

Digital Object Identifier: 10.23919/JCN.2021.000047

TABLE I
LATENCY AND RELIABILITY REQUIREMENTS FOR SELECTED INDUSTRIAL APPLICATIONS

Industrial application	**Latency** (ms)	**Reliability** (PER)
Factory automation	0.25 to 10	1×10^{-9}
Process automation	50 to 100	1×10^{-3} to 1×10^{-4}
Smart grids	3 to 20	1×10^{-6}
Intelligent transport systems	10 to 100	1×10^{-3} to 1×10^{-5}

They also fall short of meeting efficiency, reliability and latency requirements all together. [1], [7], [9].

To ensure real-time synchronization and quality of service (QoS) in industrial applications, attaining a relatively low latency without compromising reliability is paramount. For example, factory automation would require an end-to-end latency below 1ms and a reliability (PER) of 1×10^{-9}, to achieve seamless performance during control and motion of assembling lines, robots and tracking of unfinished products [2], [10]–[14]. Table I briefly describes some examples of industrial applications and their respective latency (in milliseconds) and packet error rate (PER) requirements [1], [10].

Low-latency and high reliability could be achieved through waveform design modifications, channel coding, synchronization, multiple access schemes, flexible network architecture and hardware system designs, especially at the PHY and MAC layers.

Related research has been done to achieve high performance in wireless networks through PHY layer re-modeling. For instance, in [15], a GFDM-based configuration is proposed for the packet design of intelligent transportation system (ITS)-G5-based vehicular communications to enable efficient utilization of time and frequency resources. Its performance is evaluated in terms of transmit power spectral density, PER and throughput. The realization of high-performance wireless network (WirelessHP) through minimization of the packet transmission time to reduce the inefficiencies that affect short packet transmission was proposed in [16]. In [17], authors also proposed a WirelessHP design involving a combined optimization of parameters in both the PHY and MAC layer. The size of the preamble and symbol time are reduced to achieve low latency. Another high throughput seeking GFDM-based configuration is proposed in [18], whereby a GFDM symbol without cyclic prefix (CP), but a fixed tail length equivalent to CP length is used. A GFDM frame design for IEEE 802.11ad is proposed in [19], with an objective of alleviating the high peak-to-average power ratio (PAPR) arising in the conventional OFDM designs.

Apart from [16] and [17], most of the above-mentioned

1229-2370/22/$10.00 © 2022 KICS

work does not exploit latency as a measure of network performance, a factor we deem very significant for high performance of the next generation wireless networks. Moreover, addressing latency requirements could also lead to improved throughput and subsequently achieving bandwidth efficiency [20], [21]. In this paper, motivated by the increased latency resulting from an elevated network overhead, we propose a short WLAN packet structure whose design is based on GFDM. We refer to the IEEE 802.11 WLAN standard [22]–[25] as a baseline to develop our packet structure for industrial applications because it is less costly and easy to deploy. However, it should be noted that our PHY layer does not support interoperability and backward compatibility with the existing WLAN standards. The latency and reliability requirements for our target industrial applications are 50 to 100 ms and 10^{-3} to 10^{-4} for process automation and 10 to 100 ms and 10^{-3} to 10^{-5} for intelligent transport systems. Our work can be summarized in as follows.

First, we swap the conventional OFDM-based scheme with GFDM for use in the WLAN data field. GFDM is considered because of its structure that enables allocation of cyclic prefix after every block, leading to reduced CP overhead. GFDM also requires less synchronization compared to OFDM. These properties translate into less transmission time.

Second, we reduce the preamble length from 10 symbols to 1 symbol. We assume that this length is enough for functionalities such as packet detection and synchronization [26]. Since work in an industry environment is monotonous, we assume that traffic patterns are highly predictable. This is because the time instant at which a packet arrives is well known by a given sensor or actuator node. Therefore, other features such as carrying packet information concerning modulation and coding schemes, data rate, and bandwidth can be optional since this information can be pre-set during network calibration at inception. Additionally, better receiver schemes can be implemented to achieve a performance similar to when the 10-symbol preamble is used. We then subject the resultant packet frame to an optimization algorithm to further reduce the overhead contribution by the CP, pilot, guard band and direct current (DC) subcarriers.

Finally, we apply concatenated channel coding to a modified GFDM scheme to improve reliability with tolerable complexity. In this case, self-interference and noise enhancement in the conventional GFDM are also suppressed which improves the error rate performance. Other than simulations, rigorous investigations are necessary to capture non-idealities which are not considered in this paper. Moreover, this being just our first step towards the application of GFDM to industrial wireless networks, we are in considerations of developing a prototype GFDM node for real environment testing to evaluate other features such as packet detection, channel estimation, to mention but a few.

The remaining part of this paper is organized as follows: Section II provides a review of OFDM and GFDM. Section III introduces the configuration and waveform design of the conventional GFDM and the proposed PHY layer showing how improved latency can be achieved. A noise-free GFDM configuration with suppressed self-interference and channel coding is also discussed in this section. Evaluation and simulation results are presented in section IV. Finally, a conclusion is presented in Section V.

II. System Overview

A. Overview of OFDM

OFDM is an orthogonal multicarrier modulation scheme that involves parallel transmission of a large number of closely spaced orthogonal subcarriers [27]. Through the application of CP and computationally efficient fast Fourier transform (FFT), OFDM converts a frequency-selective channel into several parallel independent frequency-flat subchannels. The mathematical expression of an OFDM symbol can be given as

$$x[n] = \frac{1}{K} \sum_{k=0}^{K-1} d_k \exp\left(j2\pi \frac{kn}{K}\right), \tag{1}$$

where $n, x[n]$ and d_k, represent the sampling index, transmitted symbol and the modulated symbol transmitted on the k-th subcarrier respectively. In (1), k is the subcarrier index while K is the total number of subcarriers. OFDM has several advantages [27], [28], such as spectral efficiency that can be achieved through dividing the spectrum into orthogonal subcarriers, low complexity receiver design which is attained through frequency domain equalization and robustness against multi-path propagation. However, OFDM harbors drawbacks [28] such as a high out-of-bound emission (OOB) as shown in Fig. 3, a high PAPR, and sensitivity to frequency and timing offsets. For those reasons, various waveform designs [29] such as filter-bank multi-carrier (FBMC), universal filter multi-carrier (UFMC), bi-orthogonal frequency division multiplexing (BFDM), and GFDM, have been proposed as potential replacements for OFDM.

B. Overview of GFDM

In this paper, we propose the use of GFDM for designing a WLAN PHY layer because of its peculiar characteristics [29] such as low OOB emissions since filtering is done at subcarrier level, and high spectrum efficiency that can be achieved through tail biting. GFDM also exhibits flexibility which makes it possible to adjust the number of subcarriers and subsymbols. Owing to the aforementioned features alongside burst transmission, GFDM is potentially capable of supporting low latency applications. GFDM is a flexible multi-carrier modulation scheme in which a number of subcarriers and subsymbols are contained in a two-dimensional block structure. Each GFDM block is independently modulated. Fig. 1 shows the frame structures of OFDM and GFDM.

Consider K subcarriers, M subsymbols and N data symbols, of which each data symbol, $d_{k,m}$ is modulated by (k, m), a pair of subcarrier and subsymbol using a pulse shaping filter $\mathrm{g}[n]$, such that $N = M \cdot K$. The resulting GFDM waveform in the time domain [29] can be expressed as

$$x[n] = \sum_{k=0}^{K-1} \sum_{m=0}^{M-1} d_{k,m} \mathrm{g}\Big[\langle n - mK \rangle_N\Big] \exp\left(-j2\pi \frac{kn}{K}\right), \tag{2}$$

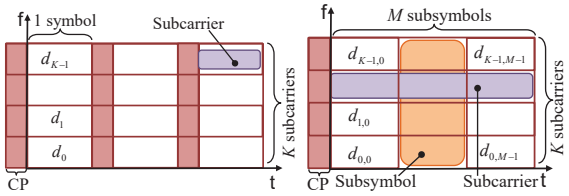

(a) OFDM (b) GFDM

Fig. 1. OFDM and GFDM frame structures

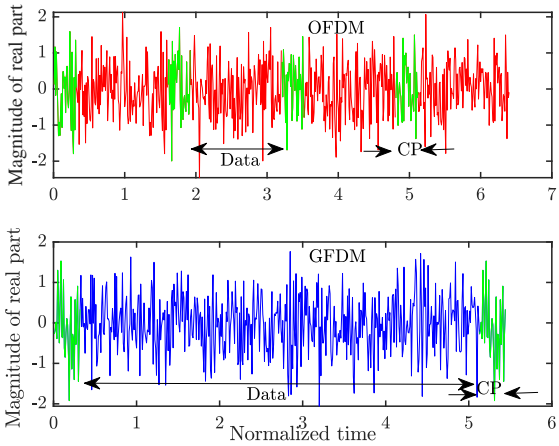

Fig. 2. Illustration of OFDM and GFDM in time domain.

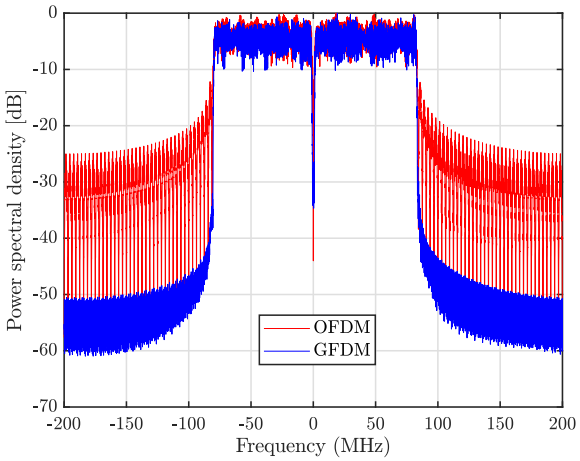

Fig. 3. OOB comparison between OFDM and GFDM.

where $g_{k,m}[n] = g[\langle n - mK \rangle_N] \exp(-j2\pi \frac{k}{K} n)$, is the cyclically shifted time and frequency version of a pulse prototype $g[n]$ with period N. In (2), $\langle \cdot \rangle_N$ represents the modulo N operation. Then we can construct (2) in vector form as

$$\mathbf{x} = \mathbf{G}\mathbf{d}, \tag{3}$$

where $\mathbf{G}$ is an $N \times N$ transmitter matrix, denoted as $\mathbf{G} = [\mathbf{g}_{0,0} \cdots \mathbf{g}_{K-1,0} \quad \mathbf{g}_{0,1} \cdots \mathbf{g}_{K-1,1} \cdots \mathbf{g}_{K-1,M-1}]$.

The matrix columns represent the filters derived from the pulse shaping filter $\mathbf{g}_{k,m} \in \mathbb{C}^{N \times 1}$, such that $\mathbf{g}_{k,m} = [g_{k,m}[0], g_{k,m}[1], \cdots, g_{k,m}[N-1]]^T$, and $\mathbf{d}$ is an $N \times 1$ data vector defined as $\mathbf{d} = [\mathbf{d}_0^T \ \cdots \ \mathbf{d}_m^T \ \cdots \ \mathbf{d}_{M-1}^T]^T$, where $\mathbf{d}_m = [d_{0,m} \quad d_{1,m} \ \cdots \ d_{K-1,m}]^T$. By adding CP to the transmit samples and taking the effect of the wireless channel into account, the received signal is given by

$$\tilde{\mathbf{y}} = \tilde{\mathbf{H}}\tilde{\mathbf{x}} + \tilde{\mathbf{w}}, \tag{4}$$

where $\tilde{\mathbf{x}}$ contains the transmit samples after adding CP, $\tilde{\mathbf{H}}$ represents the $(N + L_{\text{cp}} + L_{\text{ch}} - 1) \times (N + L_{\text{cp}})$ channel matrix derived from a channel response vector $\mathbf{h} = [h[o], h[1], \cdots, h[L_{\text{ch}} - 1]]^T$, L_{ch} is the number of channel taps and $\tilde{\mathbf{w}}$ represents additive white Gaussian noise (AWGN) with zero mean and variance σ_w^2. The received signal after removing CP can be represented as

$$\mathbf{y} = \mathbf{H}\mathbf{x} + \mathbf{w}, \tag{5}$$

where $\mathbf{H}$ is an $N \times N$ circulant matrix. The property of circular convolution allows frequency domain equalization as applied to OFDM. By performing equalization with zero forcing, the resultant received signal can be formulated as

$$\hat{\mathbf{x}} = \mathbf{H}^{-1}\mathbf{H}\mathbf{x} + \mathbf{H}^{-1}\mathbf{w} = \mathbf{x} + \hat{\mathbf{w}}. \tag{6}$$

After equalization, a $N \times N$ receiver matrix $\mathbf{R}$ is deployed to recover the transmitted data symbols as given by the expression $\hat{\mathbf{d}} = \mathbf{R}\hat{\mathbf{x}}$, where $\mathbf{R}_{\text{zf}} = \mathbf{G}^{-1}$, $\mathbf{R}_{\text{mf}} = \mathbf{G}^H$, and $\mathbf{R}_{\text{mmse}} = \left(\boldsymbol{\lambda} + \mathbf{G}^H\mathbf{G}\right)^{-1}\mathbf{G}^H$, represent zero forcing (ZF), matched filter (MF), and minimum mean square error (MMSE) detectors respectively. $\boldsymbol{\lambda}$ represents the noise covariance matrix. The ZF detector completely removes self intrinsic interference at the cost of noise enhancement. The MF detector maximizes the signal-to-noise ratio per subcarrier, but its performance deteriorates with the introduction of interference in the presence of non-orthogonal transmit pulses. The MMSE detector strikes a balance between noise enhancement and self-interference, hence giving a better performance compared to zero forcing and matched filter.

During pulse shaping, especially in the presence of a large roll-off factor for a given filter, the set of $g_{k,m}[n]$, for all k and m becomes non-orthogonal, which triggers interference in the transmission, i.e., inter-symbol interference (ISI) between $d_{k,m}$ and $d_{k,m'}$ for $m \neq m'$ and inter-carrier interference (ICI) between $d_{k,m}$ and $d_{k',m}$ for $k \neq k'$. If the effect of noise and multipath is ignored, such that the overall received signal $y[n] = x[n]$, then the received symbol at a given subcarrier can be expressed as

$$\begin{aligned}\hat{d}_{k',m'} &= \sum_{n=0}^{N-1} \mathrm{g}^{*}_{k',m'}[n]\, y[n] \\ &= \sum_{n=0}^{N-1} \mathrm{g}^{*}_{k',m'}[n] \sum_{k=0}^{K-1}\sum_{m=0}^{M-1} \mathrm{g}_{k,m}[n]\, d_{k,m} \\ &= d_{k',m'} \left(\sum_{n=0}^{N-1} \mathrm{g}^{*}_{k',m'}[n]\mathrm{g}_{k',m'}[n] \right) \\ &\quad + \underbrace{\sum_{\substack{k\neq k' \\ m\neq m'}} d_{k,m} \left(\sum_{n=0}^{N-1} \mathrm{g}^{*}_{k',m'}[n]\mathrm{g}_{k,m}[n] \right)}_{\text{Interference from other symbols}}. \end{aligned} \tag{7}$$

Generally, GFDM has shortcomings too, for instance, increased complexity of the receiver due to additional processing so as to overcome ICI and ISI introduced during pulse shaping. However, note that these can be eliminated by use of appropriate pulse shaping filters and efficient receiver schemes [29].

III. Proposed GFDM-based PHY Layer

A. Latency in the Proposed GFDM-based PHY Layer

Other than reliability, most of the existing WLAN standards do not comprehensively address the stringent latency requirements [5] in industrial networks. For example, in IEEE 802.11ax, a longer symbol duration allows for the use of a larger CP length and FFT size to improve robustness and performance in fading environments. Unfortunately, successful demodulation of closely-spaced subcarriers with the existing FFT chips is so demanding. Moreover, longer symbol times may lead to bigger drifts in timing, an error that causes ICI [30]. The price to pay is increased preamble overhead and implementation complexities which yields the latency issue.

With reference to the background from [16], we propose a PHY structure to unravel the problem of increased latency in the next generation of WLAN networks. Unlike in [16], where it is assumed that the OFDM symbols used in the preamble have the same structure as those in the data field, in this work the symbols in data field have a GFDM symbol structure. We consider GFDM because of its structure that allows allocation of cyclic prefix (CP) after every block, which leads to reduced CP overhead and hence translating into less transmission time. The preamble maintains the conventional OFDM-based configuration to ease functionalities such as synchronization. In OFDM, CP is added after every symbol, while GFDM implements CP after a block (frame) to avoid inter-frame interference, as shown in Fig. 4. The reduced size of the preamble and the resulting lower CP overhead makes it potentially possible to support latency applications. Latency T_{Lat}, in the PHY layer can be divided into five components [31] as follows

$$T_{\mathrm{Lat}} = T_{\mathrm{pac}} + T_{\mathrm{ppg}} + T_{\mathrm{ped}} + T_{\mathrm{ret}} + T_{\mathrm{prep}}, \tag{8}$$

where T_{pac} represents the time to transmit a packet, T_{ppg} is the propagation delay, T_{ped} is the time for encoding, precoding, and initial channel estimation, T_{ret} is the time for retransmission, and T_{prep} is time for preprocessing for signaling exchange.

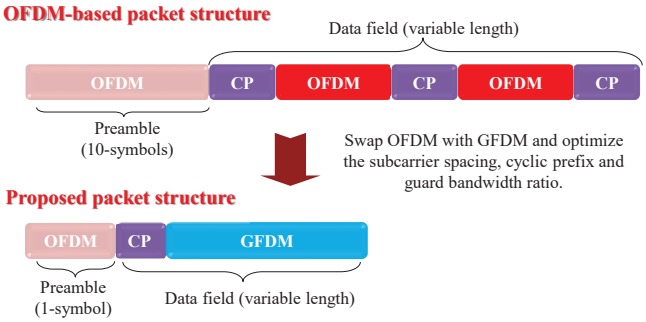

Fig. 4. Re-designing the WLAN packet structure.

It should be noted that this paper focuses on packet transmission time. However, we acknowledge that the reduction in packet transmission time does not solely lead to a latency reduction of the same magnitude since there are other components that have an impact on the overall latency. For example, propagation delay as well as processing time significantly affect latency. Since processing delay is attributed to the complexity in the waveform, by reducing the complexity, the processing delay issue can be addressed. In this case, we assume that the processing and propagation delays are negligible because we cannot control them. In wireless communications, retransmission is one of the techniques performed to improve reliability. However, a trade-off exists between latency and reliability since performing multiple retransmissions definitely leads to increased latency as in (8). We assume that T_{ret} is reduced by increasing reliability through application of a modified GFDM scheme alongside channel coding as shown in Subsections III-B and III-C.

We therefore consider T_{pac} as the main factor in determining the overall latency. The transmission time of an OFDM symbol can be defined as

$$T_{\mathrm{ofsy}} = T_{\mathrm{s}}(L_{\mathrm{cp}} + N_{\mathrm{offt}}), \tag{9}$$

where N_{offt} is the number of OFDM samples. By defining the sample time as $T_{\mathrm{s}} = 1/\beta$, it is shown that the sample time is inversely proportional to bandwidth, β. Therefore, increasing the bandwidth is significant in reducing latency. However, since bandwidth is a limited resource, we instead exploit the flexibility nature of GFDM to further reduce latency and solve the optimization problem formulated as

$$\min_{\substack{N_{\mathrm{gfft}}, \\ L_{\mathrm{cp}}, \\ N_{\mathrm{gbs}}}} \quad T_{\mathrm{s}}\Big[\underbrace{N_{\mathrm{prsy}}(L_{\mathrm{cp}} + N_{\mathrm{offt}})}_{\text{Preamble}} + \underbrace{N_{\mathrm{datsy}}(L_{\mathrm{cp}} + N_{\mathrm{gfft}})}_{\text{Payload}}\Big] \tag{10}$$

$$\text{s.t} \quad T_{\mathrm{s}} \times \Omega \geq ds_{\max}, \text{for } \Omega \in \{N_{\mathrm{gfft}}, L_{\mathrm{cp}}\}, \tag{10a}$$

$$N_{\mathrm{gbs}} \geq \eta_{\min} \times N_{\mathrm{gfft}}, \tag{10b}$$

$$N_{\mathrm{offt}} = N_{\mathrm{gfft}}. \tag{10c}$$

The minimized overall transmission time for the proposed PHY layer can be obtained from (10). In (10), N_{prsy} represents the number of symbols dedicated to the preamble while N_{datsy}

TABLE II
DESCRIPTIONS FOR SOME NOTATIONS USED IN THE PROPOSED PHY LAYER

Notation	Description
N_{offt}	OFDM samples
N_{gfft}	GFDM samples
N_{datsc}	Data subcarriers
N_{bits}	Transmitted bits
N_{pls}	Pilot subcarriers
N_{dcs}	DC subcarriers
N_{gbs}	Guard band subcarriers
N_{sts}	Spatial streams
Q	Modulation order
C_{r}	Coding rate
$ds_{\max}$	Maximum delay spread
$\lceil\cdot\rceil$	Ceiling function

is the number of symbols used for data which can be expressed as

$$N_{\text{datsy}} = \left\lceil \frac{N_{\text{bits}}}{N_{\text{datsc}} \times \log_2 Q \times C_{\text{r}} \times N_{\text{sts}}} \right\rceil, \tag{11}$$

where $N_{\text{datsc}} = N_{\text{gfft}} - (N_{\text{pls}} + N_{\text{gbs}} + N_{\text{dcs}})$.

N_{datsc} is the number of data subcarriers, N_{bits} represents the amount of data in bits to be transmitted, Q is the modulation order, C_{r} is the channel coding rate, N_{sts} is the number of spatial streams and $\lceil\cdot\rceil$ is the ceiling function. N_{gfft} represents number of samples corresponding to a GFDM block, $ds_{\max}$ is the maximum delay spread, N_{pls} represents the number of pilot subcarriers necessary for channel estimation and synchronization, N_{gbs} is the number of guard band subcarriers needed to mitigate interference from adjacent channels and N_{dcs} is the number of DC subcarriers needed to prevent the DC offsets in the desirable signal.

The constraint in (10a) involves the shortening of the subcarrier spacing (Δf) in comparison to the coherence bandwidth (β_{c}) to alleviate performance degradation caused by a long delay spread. It also calls for maintaining an appropriate CP to curb down ISI due to multipath while retaining a lower CP overhead. The constraint in (10b) necessitates determining a feasible number of guard band subcarriers to pursue an optimal guard bandwidth ratio ($\eta_{\min}$), which is defined as the ratio between the guard bandwidth ($\Delta f \times N_{\text{gbs}}$) and the total transmission bandwidth ($\Delta f \times N_{\text{gfft}}$). Guard band subcarriers should be enough to not only ensure spectral efficiency but also alleviate interference from the adjacent channels. The constraint in (10c) ensures that the number of subcarriers for both OFDM and GFDM are the same. For fair comparison, the optimization procedure is performed for both OFDM and GFDM as summarized in Algorithm 1.

Algorithm 1: Optimization algorithm

Input : $\eta_{\min}$, $ds_{\max}$, N_{dcs}, N_{psc}, N_{bits}, β
Output: T_{s}, L_{cp}, N_{gfft}, N_{datsy}, N_{datsc}

Compute the sample time, CP and coherence bandwidth $T_{\text{s}} = 1/\beta$, $T_{\text{s}} \times L_{\text{cp}} \geq ds_{\max}$, $\beta_{\text{c}} = 1/ds_{\max}$.
Find the integer θ to be used as an exponent to base 2 such that the FFT size $N_{\text{gfft}} = 2^{\theta}$, and set $\theta = 1$;
while $\{2^{\theta} \leq (ds_{\max}/T_{\text{s}}) \parallel 2^{\theta} \leq ((N_{\text{psc}}+N_{\text{dcs}})/(1-\eta_{\min}))\}$ **do**
  Compute the FFT size, $N_{\text{gfft}} = 2^{\theta}$, and the subcarrier spacing, $\Delta f = \beta/N_{\text{gfft}}$;
  if $\Delta f \leq \beta_{\text{c}}$ **then**
    Compute the number of guard subcarriers, $N_{\text{gbs}} = \eta_{\min} \times N_{\text{gfft}}$, data subcarriers, N_{datsc} and data symbols, N_{datsy};
  else
  end
  Update $\theta = \theta + 1$;
end

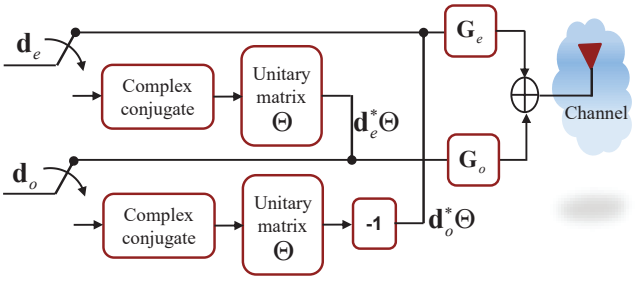

Fig. 5. CGFDM operation.

B. Suppressing Self-intrinsic Interference in GFDM

We adopt a noise-free GFDM scheme [32] and subject it to channel coding to further improve performance in the sense of reliability. The modified GFDM scheme known as coded generalized frequency division multiplexing (CGFDM), involves transmission of two-symbol blocks consecutively. As shown in Fig. 5, the data stream and transmitter matrix are divided into even and odd portions, i.e., $\mathbf{d}_{\text{e}}$ and $\mathbf{d}_{\text{o}}$ each of size $N \times 1$ for data symbols, while $\mathbf{G}_{\text{e}}$ and $\mathbf{G}_{\text{o}}$ are of size $N \times N$ each for the CGFDM transmitter matrix. The time-domain representation of the transmitted stream can be expressed as

$$x[n] = \sum_{k=0}^{K-1} \sum_{m=0}^{2M-1} d_{k,m} g_{k,m}[n], \quad \text{for} \quad n = 0, \cdots, N-1. \tag{12}$$

It should be noted that during pulse shaping in the conventional GFDM, time domain shifting is by K while in CGFDM, it is by $K/2$. Then the pulse shaping filter $\text{g}[n]$ can be given as

$$\text{g}_{k,m}[n] = \text{g}\left[\langle n - mK/2 \rangle_N\right] \exp\left(-j2\pi \frac{k}{K} n\right). \tag{13}$$

Note that for CGFDM, the overall transmitter matrix $\mathbf{G}$ is of size $N \times 2N$. From (5), the received vector streams for the first and second block transmission can be formulated as

$$\mathbf{y}_1 = \frac{1}{\sqrt{2}} \mathbf{H} \left(\mathbf{G}_{\text{e}} \mathbf{d}_{\text{e}} + \mathbf{G}_{\text{o}} \mathbf{d}_{\text{o}}\right) + \mathbf{w}_1, \tag{14}$$

and

$$\mathbf{y}_2 = \frac{1}{\sqrt{2}} \mathbf{H} \left(-\mathbf{G}_{\text{e}} \mathbf{\Theta} \mathbf{d}_{\text{o}}^{*} + \mathbf{G}_{\text{o}} \mathbf{\Theta} \mathbf{d}_{\text{e}}^{*}\right) + \mathbf{w}_2, \tag{15}$$

respectively, where $\mathbf{G}_{\mathrm{e}}$ and $\mathbf{G}_{\mathrm{o}}$ are given as $\mathbf{G}_{\mathrm{e}} = \sqrt{2}[\mathbf{G}_0, \mathbf{G}_2, \cdots, \mathbf{G}_{2M-2}]$, and $\mathbf{G}_{\mathrm{o}} = \sqrt{2}[\mathbf{G}_1, \mathbf{G}_3, \cdots, \mathbf{G}_{2M-1}]$, while $\mathbf{d}_{\mathrm{e}}$ and $\mathbf{d}_{\mathrm{o}}$ are denoted as $\mathbf{d}_{\mathrm{e}} = [\mathbf{d}_0^T, \mathbf{d}_2^T, \cdots, \mathbf{d}_{2M-2}^T]^T$ and $\mathbf{d}_{\mathrm{o}} = [\mathbf{d}_1^T, \mathbf{d}_3^T, \cdots, \mathbf{d}_{2M-1}^T]^T$. In (15), $\boldsymbol{\Theta}$ represents the $N \times N$ unitary matrix defined as

$$\boldsymbol{\Theta} \triangleq \begin{bmatrix} 0 & & 1 \\ & \iddots & \\ 1 & & 0 \end{bmatrix}. \tag{16}$$

By concatenating (14) and (15), the overall received vector after removal of CP can be constructed as

$$\underbrace{\begin{bmatrix} \mathbf{y}_1 \\ \mathbf{y}_2^* \end{bmatrix}}_{\mathbf{y}} = \frac{1}{\sqrt{2}} \underbrace{\begin{bmatrix} \mathbf{H} & \mathbf{0}_N \\ \mathbf{0}_N & \mathbf{H}^* \end{bmatrix}}_{\boldsymbol{\rho}} \begin{bmatrix} \mathbf{G}_{\mathrm{e}} & \mathbf{G}_{\mathrm{o}} \\ \mathbf{G}_{\mathrm{o}}^* \boldsymbol{\Theta} & -\mathbf{G}_{\mathrm{e}}^* \boldsymbol{\Theta} \end{bmatrix} \underbrace{\begin{bmatrix} \mathbf{d}_{\mathrm{e}} \\ \mathbf{d}_{\mathrm{o}} \end{bmatrix}}_{\mathbf{d}} + \underbrace{\begin{bmatrix} \mathbf{w}_1 \\ \mathbf{w}_2^* \end{bmatrix}}_{\mathbf{w}}. \tag{17}$$

The received signal can further be represented as

$$\mathbf{y} = \boldsymbol{\rho} \boldsymbol{\Phi} \mathbf{d} + \mathbf{w}, \tag{18}$$

where $\boldsymbol{\Phi} = \frac{1}{\sqrt{2}} \begin{bmatrix} \mathbf{G}_{\mathrm{e}} & \mathbf{G}_{\mathrm{o}} \\ \mathbf{G}_{\mathrm{o}}^* \boldsymbol{\Theta} & -\mathbf{G}_{\mathrm{e}}^* \boldsymbol{\Theta} \end{bmatrix}$ represents the effective transmitter matrix, which exhibits a unitary property such that $\boldsymbol{\Phi}^H \boldsymbol{\Phi} = \mathbf{I}_{2N}$. The desired symbols can be recovered by deploying a matched filter using the expression $\hat{\mathbf{d}} = \mathbf{R}_{\mathrm{mf}} \mathbf{y}$, where $\mathbf{R}_{\mathrm{mf}} = \boldsymbol{\Phi}^H \boldsymbol{\rho}^{-1}$.

C. Improving Reliability in the Proposed Layer

We also propose the use of error correction and detection schemes to boost performance. In communication systems, the main error control techniques include automatic repeat request (ARQ), forward error control (FEC) and hybrid automatic repeat request (HARQ). HARQ is a combination of ARQ and FEC. ARQ constitutes conducting multiple retransmissions in case of detection of errors in the received packets whereas FEC is performed by adding redundancy to the transmitted signal to enhance error detection and correction [33], [34].

To improve reliability without jeopardizing latency, we deploy forward error control (FEC), in particular, Reed-Solomon (RS), convolutional (CC) and Bose-Chaudhuri-Hocquenghem (BCH) codes. In modern communication systems much better codes such as low-density parity check (LDPC), polar and turbo are also deployed. However, these generally have longer lengths, complex encoding and decoding, and higher processing latency, especially when used for short packet communications [34], [35]. We therefore exploit concatenation of codes to achieve better performance with lower complexity, i.e., concatenating RS with BCH (RS+BCH) and RS with CC (RS+CC) [36].

We consider a BCH($N_{\mathrm{bch}}, K_{\mathrm{bch}}$) code defined over Galois field GF(2^γ) with a symbol length of γ bits, in which $N_{\mathrm{bch}} = 2^\gamma - 1$ is the code length and the message length $K_{\mathrm{bch}} = N_{\mathrm{bch}} - 2\gamma$. Additionally, a RS($N_{\mathrm{rs}}, K_{\mathrm{rs}}$) and a CC($R_{\mathrm{cc}}$) are also considered. $R_{\mathrm{rs}}, R_{\mathrm{cc}}$ and R_{bch} represent the coding rate for RS, CC and BCH codes respectively. The overall coding rate can be defined as $R_{\mathrm{rs}} \times R_{\mathrm{cc}}$ for RS+CC, while $R_{\mathrm{rs}} \times R_{\mathrm{bch}}$ for RS+BCH. RS code originally set as RS(255,239) is shortened to RS(255,223) and the resulting RS coding rate expressed as $S_{\mathrm{rs}}/(N_{\mathrm{rs}} - (K_{\mathrm{rs}} - S_{\mathrm{rs}}))$. $S_{\mathrm{rs}} = 223$, represents the new message length. The BCH code is set as BCH(63,36) while the CC is set to CC(3/4) with a generator polynomial [171 133] in octal and a constraint length of 7. The coding rate 3/4 is achieved by puncturing the bits of CC(1/2). Note that RS is used as an inner code for all concatenation cases, while CC and BCH codes are outer codes. At the transmitter side, input bits are arranged in a group of γ-bit symbols, zero padded and encoded by the RS encoder. The output of the RS encoder is also zero padded and then fed to either CC or BCH encoders. The resultant encoded sequence undergoes modulation and it is transmitted over the wireless channel. At the receiver side, the steps done during transmission are reversed to recover the transmitted bits. All encoding and decoding simulations are done in matlab. Viterbi algorithm is used for decoding CC while Berlekamp-Massey algorithm is applied to RS and BCH [34].

IV. Numerical Results

In our simulations, we consider the payload size, bandwidth requirement, modulation order and PER as metrics for performance evaluation. We consider single-input single-output (SISO, 1×1) and multiple-input multiple-output (MIMO, 2×2) transmissions under 2.4 and 5 GHz bands. We also consider operating under a worst case scenario and therefore adopt the channel model F [22] as described in Table III to replicate the highly reflective environment in an industry, such as process automation and intelligent transport systems, which are our target industrial applications. For latency evaluation, without any coding ($C_{\mathrm{r}} = 1$), the number of DC subcarriers and spatial streams is set to $N_{\mathrm{dcs}} = 1$ and $N_{\mathrm{sts}} = 1$, respectively. We consider $M = 5$ for GFDM since it provides a better performance in terms of trade-off between packet transmission time and symbol error rate. Table IV shows the parameters used to obtain the following results.

Fig. 6 illustrates the performance comparison between the OFDM and GFDM-based PHY layer with varying bandwidth for BPSK and 8-PSK modulation schemes[1]. Under both BPSK and 8-PSK, it is shown that the packet transmission time decreases with increase in bandwidth. Moreover MIMO boosts the overall performance. For instance, under BPSK, performance is improved by 72% and 68% at 80 and 160 MHz respectively. This means that having a high bandwidth necessitates a higher FFT size which leads to a smaller subcarrier spacing, hence, all the data bits can be carried by fewer number of symbols. Consequently, the reduction in sample time by increased bandwidth has a great impact on the transmission time. Additionally, Fig. 6 also shows the impact of varying the modulation order on the packet transmission time. In this case, $Q = \{2, 8\}$ for BPSK and 8-PSK respectively. The results show that as the modulation order increases the packet transmission time reduces. For example, at 20 MHz, the packet transmission time of the MIMO GFDM-based PHY

[1]We verify that other modulations follow a similar trend to Fig. 6, which is not shown in this paper.

TABLE III
CHANNEL MODEL F DELAY TAPS AND GAIN

Tap index	1	2	3	4	5	6	7	8	9	10	11	12	13	14	15	16	17	18
Power [dB]	-3.3	-3.6	-3.9	-4.2	-1.8	-2.8	-3.5	-4.4	-5.7	-6.7	-10.4	-9.6	-8.8	-13.3	-12.9	-14.2	-16.3	-21.2
Excess delay [ns]	0	10	20	30	50	80	110	140	180	230	280	330	400	490	600	730	880	1050

TABLE IV
SIMULATION PARAMETERS

Parameter	**OFDM**	**GFDM**	**CGFDM**
Subsymbols (M)	1	5	
Prototype filter	Rect	RRC	
Roll-off		0.5	
Preamble symbols	1		
Subcarriers (K)	64, 256, 512, 1024, 2048		
Cyclic prefix	32, 64, 128, 256, 512		
Maximum delay spread [ns]	400, 800		
Guard bandwidth ratio	0.1875		
Bandwidth [MHz]	20, 40, 80, 160		
Modulation order	2, 4, 8, 16		

layer is approximately 120 and 40 μs for BPSK and 8-PSK respectively. Availability of bandwidth alongside higher-order modulation schemes support high data rates, hence, more data bits are transmitted per symbol. This performance shows that the use of high-order modulation will be significant in the future WLANs standards, not only at improving data rates but also lowering latency.

Fig. 7 depicts the packet transmission time versus payload (data) size for 20 and 80 MHz bandwidth[2]. The figure indicates that as the payload size increases, so does the overall packet transmission time. For example, at 80 MHz under SISO transmission, the latency gap between OFDM and GFDM increases by 40%. This results from the redundancy introduced by an increased CP overhead. MIMO presents 67% and 72% improvement in latency for 75 and 125 bytes respectively. Data is transmitted over two spatial streams which results into improved data rates. By comparing 20 MHz to 80 MHz bandwidth, it is shown that latency significantly reduces as the bandwidth increases, which is as a result of support for higher data rates.

Fig. 8 compares the PER performance of CGFDM with OFDM and GFDM under AWGN and channel model F. This figure shows that CGFDM outperforms the conventional GFDM under AWGN. Interference, noise enhancement and the choice of roll-off factor in GFDM are the reasons for having a higher PER in GFDM. However, CGFDM achieves the same performance as OFDM. Since CGFDM utilizes a unitary self-interference matrix, there is complete removal of interference and no added noise enhancement. Fig. 8 also shows that CGFDM outperforms both OFDM and GFDM under channel model F since it exhibits a better spectrum resolution under frequency selective channels.

Fig. 9 shows the impact of ISI and ICI on the PER performance of uncoded OFDM, GFDM, and CGFDM due to the channel. The loss of orthogonality in time domain due to ISI is as a result of delay spread whereas loss of orthogonality in frequency domain due to ICI is caused by doppler effects.

[2]We verify that other sizes of bandwidth follow a similar trend to Fig. 7, which is not shown in this paper.

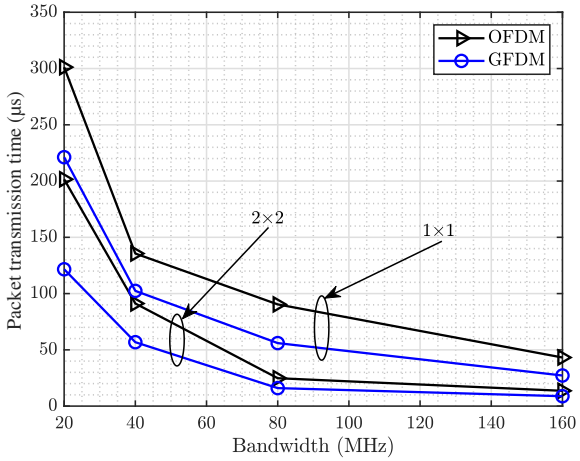

(a)

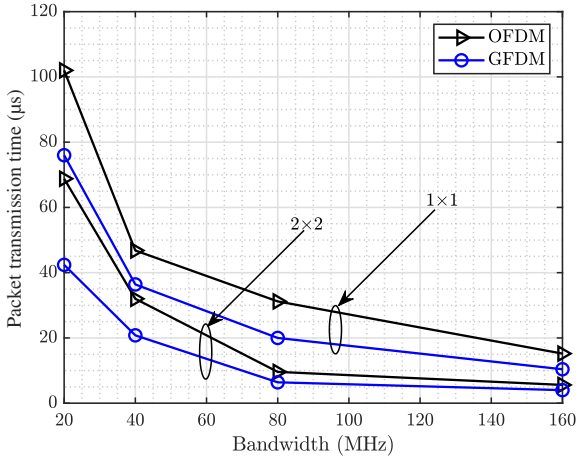

(b)

Fig. 6. Packet transmission time against bandwidth for OFDM and GFDM-based PHY layers with $M = 5$, $N_{\text{bits}} = 1000$ and $Q = \{2, 8\}$: (a) BPSK and (b) 8-PSK respectively, under SISO and MIMO transmission at a PER of order 10^{-2} for uncoded systems.

In Fig. 9, it is shown that for short CP length, ISI and ICI are dominant, which leads to a very poor performance when channel model F is used. This is well illustrated by the performance of CGFDM when CP = 6 in comparison to CP = 28. For all varying cases of CP, CGFDM performs best at lower SNR compared to OFDM and GFDM. However, when CP =6, OFDM performs better than CGFDM and GFDM. GFDM and CGFDM are both block-based multicarrier systems which deploy a single CP per frame. Therefore, in presence of ISI and ICI with insufficient CP length, all data in a single block gets corrupted at once leading to deterioration in performance. Additionally, as described in II-B, the matched filter exhibits the worst performance especially at high SNR. In this case

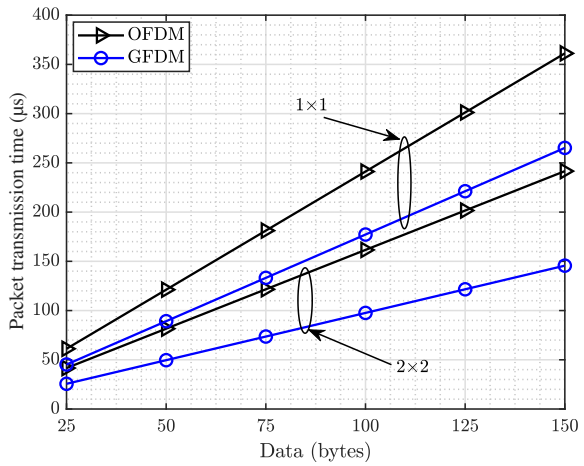

Fig. 7. Packet transmission time versus payload for OFDM and GFDM-based PHY layers under SISO and MIMO transmission with $M = 5$, $Q = 2$ and $\beta = \{20, 80\}$MHz for (a) and (b) respectively at a PER of order 10^{-2} .

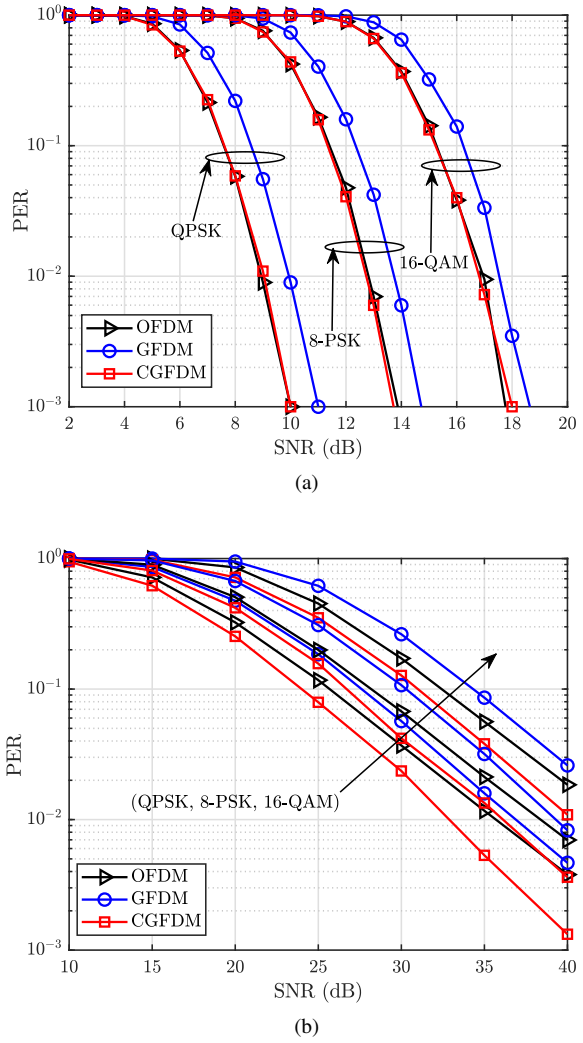

Fig. 8. PER performance for uncoded CGFDM, GFDM and OFDM under (a) AWGN and (b) channel model F with 16-QAM, $K = 64$, $M = 5$ and and a RRC filter of roll-off factor, $\alpha = 0.5$ at a packet transmission time of about 25.3μs.

OFDM has advantage over CGFDM since it deploys a zero forcing filter.

Fig. 10 illustrates the PER performance of the concatenated RS with BCH (RS+BCH) coding for CGFDM and OFDM under AWGN and channel model F. This figure indicates that CGFDM has a performance similar to OFDM for non-concatenated codes (RS, BCH) due to absence of noise enhancement and interference in CGFDM under AWGN. However, OFDM lags CGFDM by a difference of about 1.1 dB when subjected to concatenated codes (RS+BCH). CGFDM performs better than OFDM since it utilizes a unitary matrix which makes it more immune to errors introduced by the process of concatenation. Moreover, codes such as RS are vulnerable to random errors due to the channel. Under channel model F, OFDM performance deteriorates due to spectral resolution discrepancy compared to that of CGFDM. Fig. 10 also shows that concatenating codes improves the performance under both AWGN and channel model F. For instance, the concatenated RS with BCH code approaches a PER of order 10^{-3} at about 9 and 7.9 dB SNR for OFDM and CGFDM respectively under AWGN, which results into a 4.98 and 6.08 dB gain respectively. However, the same PER under channel model F is attained at about 32.7 and 29.8 dB for OFDM and CGFDM respectively which leads to a coding gain of about 32.3 and 26.2 dB respectively. Nevertheless, the coding gain exhibited by OFDM is not enough to overturn the overall performance of CGFDM. Generally, the combination of RS and BCH leads to an improvement in performance as a result of random and burst error correction capability boost under AWGN and channel model F respectively.

Fig. 11 portrays the PER performance of the concatenated RS with CC coding for OFDM and CGFDM under AWGN and channel model F. The figure shows that under non-concatenated codes (RS, CC), OFDM and CGFDM exhibit a similar performance under AWGN. However, due to stronger error immunity, CGFDM leads OFDM by a gain of about 0.8 dB when subjected to concatenated coding (RS+CC). By concatenating RS with CC (RS+CC) code under AWGN, a PER of order 10^{-3} is approached at about 8.7 and 7.9 dB

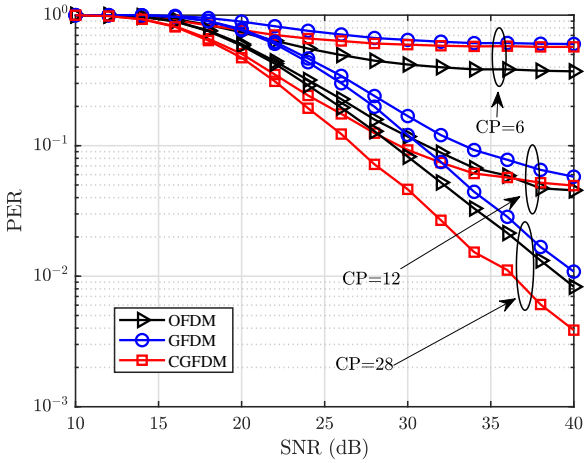

Fig. 9. Impact of ISI and ICI due to channel model F on the error performance with 16-QAM, $K = 40$, $M = 5$, CP = $\{6, 12, 28\}$ and a RRC filter of roll-off factor, $\alpha = 0.5$ at a packet transmission time of about 25.3 μs.

SNR for OFDM and CGFDM respectively, which translates into a coding gain of 5.28 and 6.08 dB respectively. However, under channel model F, the same PER is attained at 30 and 28.8 dB for OFDM and CGFDM respectively. Consequently, a coding gain of about 35 and 27.2 dB is achieved by OFDM and CGFDM respectively. In this case, the repercussion of CC decoding lies in the introduction of burst errors. These greatly affect the performance of the CC code. A doubly improved error correction capability for random errors by CC codes and burst errors by RS codes occurs due to applied concatenation of RS with CC.

V. Conclusion

In this paper, the performance of the GFDM scheme was investigated for implementation in WLANs in order to support industrial applications. Re-modeling of the conventional OFDM-based WLAN PHY layer was proposed, in which the data field was modified and the packet length downsized. The results show that the overall packet transmission time was reduced, which emphasizes a lower latency. For clarity, the results presented are for optimized cases of OFDM and GFDM-based PHY layers, otherwise, an unoptimized OFDM-based PHY layer performs worse than the optimized one. The optimized GFDM-based configuration outperforms OFDM with a reduced latency of about 40% to 72% under SISO and MIMO transmissions. Despite GFDM being more computationally complex than OFDM, it can achieve a similar performance such as PER, due to its flexibility as shown in the obtained results. Moreover, the cost of increased complexity and PER can be compensated by using appropriate pulse shaping filters and advanced receiver techniques. By deploying channel coding, we have also shown that it is possible to achieve reliability of order 10^{-3} which is a minimum requirement for our target industrial applications namely, process automation and intelligent transport systems. However, it would be more beneficial to achieve higher reliability than the one obtained in this paper through applying other techniques such as, spatial diversity schemes, enhanced synchronization,

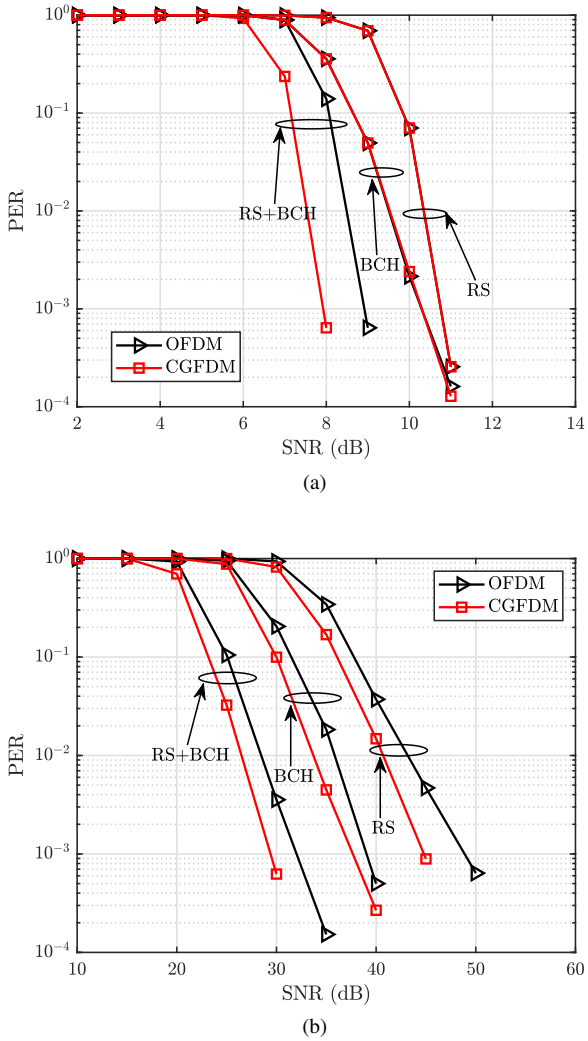

Fig. 10. PER performance for CGFDM and OFDM when subjected to concatenated RS(255,223) + BCH(63,36) coding under: (a) AWGN and (b) channel model F with 16-QAM, $K = 256$, $M = 5$ and a RRC filter of roll-off factor, $\alpha = 0.5$ at a packet transmission time of about 25.3 μs.

and beamforming altogether. The attained performance can be suitable for applications such as process automation and intelligent transport systems, and hence rendering the proposed PHY configuration a benchmark for development of wireless networks for latency-critical industrial applications. The work presented in this paper reflects the first stride we have taken towards the application of GFDM to industrial networks to attain low latency and high reliability. We are in consideration of performing rigorous real environment experiments by developing a fully functional prototype GFDM node as part of our future work. This would be possible by deploying field programmable array (FPGA)-based hardware such as software defined radio (SDR). The transmitter and receiver programs for generation and detection of the GFDM packet would be designed using dedicated software such as LabVIEW programming language [37], [38].

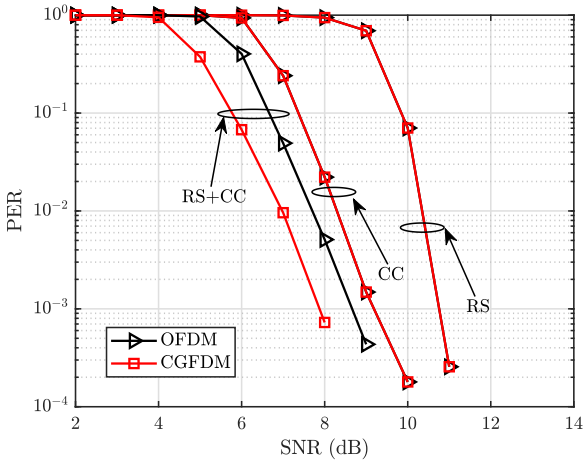

(a)

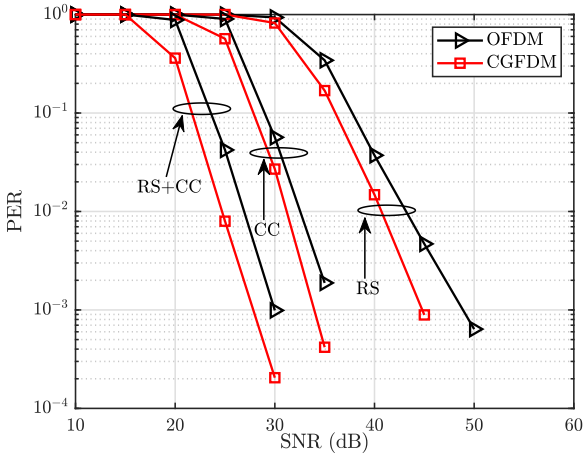

(b)

Fig. 11. PER performance for CGFDM and OFDM when subjected to concatenated RS(255,223) + CC(3/4) coding under: (a) AWGN and (b) channel model F with 16-QAM, $K = 256$, $M = 5$ and a RRC filter of roll-off factor, $\alpha = 0.5$ at a packet transmission time of about 25.3 μs.

REFERENCES

[1] P. Schulz *et al.*, "Latency critical IoT applications in 5G: Perspective on the design of radio interface and network architecture," *IEEE Commun. Mag.*, vol. 55, no. 2, pp. 70–78, Feb. 2017.

[2] Z. Pang, M. Luvisotto, and D. Dzung, "Wireless high-performance communications: The challenges and opportunities of a new target," *IEEE Trans. Ind. Electron. Mag.*, vol. 11, no. 3, pp. 20–25, Sep. 2017.

[3] V. C. Gungor *et al.*, "Smart grid technologies: Communication technologies and standards," *IEEE Trans. Ind. Informat.*, vol. 7, no. 4, pp. 529–539, Nov. 2011.

[4] M. Gerla, E. Lee, G. Pau, and U. Lee, "Internet of vehicles: From intelligent grid to autonomous cars and vehicular clouds," in *Proc. IEEE WF-IoT*, 2014.

[5] X. Jiang *et al.*, "Low-latency networking: Where latency lurks and how to tame it," *Proc. IEEE*, vol. 107, no. 2, pp. 280–306, Feb. 2019.

[6] P. Ramezani and A. Jamalipour, "Toward the evolution of wireless powered communication networks for the future Internet of things," *IEEE Netw.*, vol. 31, no. 6, pp. 62–69, Nov./Dec. 2017.

[7] M. Centenaro, L. Vangelista, A. Zanella, and M. Zorzi, "Long-range communications in unlicensed bands: The rising stars in the IoT and smart city scenarios," *IEEE Wireless Commun.*, vol. 23, no. 5, pp. 60–67, Oct. 2016.

[8] Cisco. IEEE 802.11ax: The sixth generation of Wi-Fi. [Online]. Available: https://www.cisco.com/c/en/us/products/collateral/wireless/white-paper-c11-740788.html

[9] I. Selinis, *et al.*, "The race to 5G era; LTE and Wi-Fi," *IEEE Access*, vol. 6, pp. 56598–56636, Oct. 2018.

[10] B. Holfeld *et al.*, "Wireless communication for factory automation: An opportunity for LTE and 5G systems," *IEEE Commun. Mag.*, vol. 54, no. 6, pp. 36–43, Jun. 2016.

[11] A. Willig, K. Matheus, and A. Wolisz, "Wireless technology in industrial networks," *Proc. IEEE*, vol. 93, no. 6, pp. 1130–1151, Fig. Jun. 2005.

[12] M. Luvisotto, Z. Pang, and D. Dzung, "Ultra high performance wireless control for critical applications: challenges and directions," *IEEE Trans. Ind. Informat.*, vol. 13, no. 3, pp. 1448–1459, Jun. 2017.

[13] M. Bennis, M. Debbah, and H. V. Poor, "Ultrareliable and low-latency wireless communication: Tail, risk, and scale," *Proc. IEEE*, vol. 106, no. 10, pp. 1834–1853, Oct. 2018.

[14] K. S. Kim *et al.*, "Ultrareliable and low-latency communication techniques for tactile internet services," *Proc. IEEE*, vol. 107, no. 2, pp. 376–393, Feb. 2019.

[15] D. Zhang, A. Festag, and G. P. Fettweis, "Performance of generalized frequency division multiplexing based physical layer in vehicular communications," *IEEE Trans. Veh. Technol.*, vol. 66, no. 11, pp. 9809–9824, Nov. 2017.

[16] M. Luvisotto, *et al.*, "Physical layer design of high-performance wireless transmission for critical control applications," *IEEE Trans. Ind. Informat.*, vol. 13, no. 6, pp. 2844–2854, Dec. 2017.

[17] M. Luvisotto, Z. Pang, and D. Dzung, "High-performance wireless networks for industrial control applications: New targets and feasibility," *Proc. IEEE*, vol. 107, no. 6, pp. 1074–1093, Jun. 2019.

[18] A. Nimr, D. Zhang, A. Martinez, and G. Fettweis, "A study on the physical layer performance of GFDM for high throughput wireless communication," in *Proc. EUSIPCO*, 2017.

[19] H. Shimodaira, J. Kim, and A. S. Sadri, "Enhanced next generation millimeter-wave multicarrier system with generalized frequency division multiplexing," *Int. J. Antennas Propag.*, vol. 2016, no. 9269567, Dec. 2016.

[20] B. Soret, P. Mogensen, K. I. Pedersen, and M. C. Aguayo-Torres, "Fundamental trade-offs among reliability, latency and throughput in cellular networks," in *Proc. IEEE GLOBECOM Workshops*, Dec. 2014.

[21] J. Padhye, V. Firoiu, D. F. Towsley, and J. F. Kurose, "Modeling TCP Reno performance: A simple model and its empirical validation," *IEEE/ACM Trans. Netw.*, vol. 8, no. 2, pp. 133–145, Apr. 2000.

[22] E. Perahia and R. Stacey, *Next generation wireless LANs: 802.11 n and 802.11 ac*. Cambridge university press, 2013.

[23] *IEEE 802.11ax Channel Model Document*, IEEE 802.11-14/0882r4, 2014.

[24] R. Stacey, "IEEE 802.11ax Specification Frame work of TGax Document, doc.: IEEE 802.11-15/0132r15, January 2016,," https://mentor.ieee.org/802.11/dcn/15/11-15-0132-17-00ax-spec-framework.docx, Accessed: 11-2-2020.

[25] *IEEE standard for information technology—telecommunications and information exchange between systems local and metropolitan area networks—specific requirements - Part 11: Wireless LAN medium access control (MAC) and physical layer (PHY) specifications*, IEEE Std 802.11-2016 (Revision of IEEE Std 802.11-2012), 2016.

[26] X. Jiang, *et al.*, "Packet detection by a single ofdm symbol in urllc for critical industrial control: A realistic study," *IEEE J. Sel. Areas Commun.*, vol. 37, no. 4, pp. 933–946, Apr. 2019.

[27] J. A. C. Bingham, "Multicarrier modulation for data transmission: An idea whose time has come," *IEEE Commun. Mag.*, vol. 28, no. 5, pp. 5–14, May 1990.

[28] E. Dahlman, S. Parkvall, and J. Skold, *4G: LTE/LTE-advanced for mobile broadband*. Academic press, 2013.

[29] N. Michailow *et al.*, "Generalized frequency division multiplexing for 5th generation cellular networks," *IEEE Trans. Commun.*, vol. 62, no. 9, pp. 3045–3061, Sep. 2014.

[30] Rohde & Schwarz. (2016) IEEE 802.11ax Technology Introduction. [Online]. Available: http://resources.rohde-schwarz-usa.com/c/1-ma222-0e-ieee80211

[31] H. Ji, *et al.*, "Ultra-reliable and low-latency communications in 5g downlink: physical layer aspects," *IEEE Wireless Commun.*, vol. 25, no. 3, pp. 124–130, Jun. 2018.

[32] M. Towliat and S. M. J. Asgari Tabatabaee, "GFDM interference mitigation without noise enhancement," *IEEE Commun. Lett.*, vol. 22, no. 5, pp. 1042–1045, May 2018.

[33] Y. H. Yitbarek, *et al.*, "Implementation and evaluation of error control schemes in industrial wireless sensor networks," in *Proc. IEEE ICIT*, 2014.

[34] G. C. Clark Jr and J. B. Cain, *Error-correction coding for digital communications*. Springer Science & Business Media, 2013.
[35] M. Shirvanimoghaddam *et al.*, "Short block-length codes for ultra-reliable low latency communications," *IEEE Commun. Mag.*, vol. 57, no. 2, pp. 130–137, Feb. 2019.
[36] G. Forney, *Concatenated codes (research monograph)*, MA: MIT Press, 1966.
[37] M. Danneberg *et al.*, "Universal waveforms processor," in *Proc. EuCNC*, 2018.
[38] M. Danneberg *et al.*, "Flexible transceiver implementation," http://owl.ifn.et.tu-dresden.de/GFDM/, Accessed: 20-5-2020.

Julius Ssimbwa received the B.S. degree in Telecommunications Engineering from Makerere University, Kampala, Uganda, in 2016, and the M.S. degree in Electrical Engineering from Korea University, Seoul, Korea, in 2021. He is currently pursuing the Ph.D. degree at Korea University. He was an O&M Engineer at Huawei Technologies (Uganda) from 2015 to 2016. In 2017, he joined I-Engineering group (Uganda) as an O&M Supervisor. His current research interests are signal processing and resource allocation in wireless networks.

Byungju Lim received the B.S. and Ph.D. degrees in Electrical Engineering from Korea University, Seoul, Korea in 2015 and 2021, respectively. He is currently a Post-Doctoral Fellow with the Korea University. His current research interests include machine learning and signal processing for wireless communication.

Young-Chai Ko received the B.Sc. degree in electrical and Telecommunication Engineering from the Hanyang University, Seoul, Korea and the M.S.E.E. and Ph.D. degrees in Electrical Engineering from the University of Minnesota, Minneapolis, MN in 1999 and 2001, respectively. He was with Novatel Wireless as a research scientist from January 2001 to March 2001. In March 2001, he joined the Texas Instruments, Inc., Wireless Center, San Diego, CA, as a Senior Engineer. He is now with the school of Electrical Engineering at Korea University as a Professor. His current research interests include the design and evaluations of multi-user cellular system, MODEM architecture, mm-wave and Tera Hz wireless systems.